Available online at www.sciencedirect.com
ScienceDirect
Trans. Nonferrous Met. Soc. China 29(2019) 1057−1066
Transactions of Nonferrous Metals Society of China
www.tnmsc.cn

Microstructure, hydrogen storage thermodynamics and kinetics of $La_5Mg_{95-x}Ni_x$ (x=5, 10, 15) alloys

Zhen-yang LI[1,2], Sheng-li LI[1], Ze-ming YUAN[2,3], Yang-huan ZHANG[2,3], Yan QI[2]

1. School of Materials Science and Engineering, Shandong University, Ji'nan 250061, China;
2. Department of Functional Material Research, Central Iron and Steel Research Institute, Beijing 100081, China;
3. Key Laboratory of Integrated Exploitation of Baiyun Obo Multi-Metal Resources, Inner Mongolia University of Science and Technology, Baotou 014010, China

Received 27 June 2018; accepted 30 December 2018

Abstract: The microstructure, hydrogen storage thermodynamics and kinetics of $La_5Mg_{95-x}Ni_x$ (x=5, 10, 15) ternary alloys with different Ni contents were investigated. The evolutions of the microstructure and phase of experimental alloys were characterized by X-ray diffractometry and scanning electron microscopy. The hydrogen storage kinetics and thermodynamics, and P−C−I curves were tested using a Sievert apparatus. It is found that increasing Ni content remarkably improves hydrogen storage kinetics but reduces the hydrogen storage capacity of alloys. The highest hydrogen absorption/desorption rate is observed in the $La_5Mg_{80}Ni_{15}$ alloy, with the lowest hydrogen desorption activation value being 57.7 kJ/mol. By means of P−C−I curves and the van't Hoff equation, it is determined that the thermodynamic performance of the alloy is initially improved and then degraded with increasing Ni content. The $La_5Mg_{85}Ni_{10}$ alloy has the best thermodynamics properties with a hydrogenation enthalpy of −72.1 kJ/mol and hydrogenation entropy of −123.2 J/(mol·K).

Key words: hydrogen storage; Mg-based alloys; thermodynamics performance; kinetics performance; Ni content

1 Introduction

Hydrogen energy is a clean, efficient, safe, abundant, and sustainable secondary energy [1−3], and hydrogen storage technology is the critical aspect of hydrogen energy development and application. Hydrogen storage refers to the methods and equipment to confine hydrogen in a certain form (molecular, atomic, or ionic states) within a volume and mass that fit the actual application and achieve a suitable volumetric and mass energy density [4,5]. Globally, the application of hydrogen energy is considered to be critical. One of the 10 major scientific developments in China in 2017 was the realization of cryogenic preparation and storage of hydrogen. Mg and Mg-based alloys have become attractive hydrogen storage materials because of their high hydrogen capacity (7.6 wt.% for MgH_2, 3.6 wt.% for Mg_2NiH_4) and abundant reserves [6]. Nevertheless, hydrogen storage has many problems, including high dehydrogenation temperature, sluggish hydrogen storage kinetic performance, and poor electrochemical cycle stability that seriously affect its practical development [7,8].

In 1980, OESTERREICHER and RITTNER [9] introduced the $La_{1-x}Mg_xNi_2$ alloy using the induction melting method, which introduced the hydrogen storage research field to the study of RE−Mg−Ni-based materials. $La_{0.33}Mg_{0.67}Ni_2$ compounds can form hydrides at room temperature. Related studies revealed that Re−Mg−Ni alloys have good capacities and excellent hydrogen absorption/ desorption properties [10−13]. For example, ZHANG et al [14] comprehensively reported that the melt-spun $Mg_{10}NiLa$ specimens show an amorphous phase and minor crystalline La_2Mg_{17} after melt spinning. KALINICHENK et al prepared $Mg_{90}Ni_8RE_2$ (RE=Y, Nd, Gd) and melt-spun Mg−Ni−Cu−Y and obtained hydrogen storage and absorption capacities of 5.6 [15] and 4.8 wt.% [16], respectively. They also prepared $Mg_{80}Ni_{10}Y_{10}$ and obtained a reversible hydrogen capacity

Foundation item: Projects (51761032, 51471054) supported by the National Natural Science Foundation of China
Corresponding author: Yang-huan ZHANG, Tel: +86-10-62183115, Fax: +86-10-62187102, E-mail: zhangyh59@sina.com; Sheng-li LI, Tel: +86-531-88395620, Fax: +86-531-8392313, E-mail: lishengli@sdu.cn
DOI: 10.1016/S1003-6326(19)65014-4

of 5.2 wt.% [17]. HAO et al [18] prepared $Mg_{88.5}Ni_xLa_y$ (y/x=1/16) alloys and obtained a hydrogen storage capacity of 4.45 wt.%. LV et al [19] reported on the microstructural evolution of Mg−xNi−3La (x=5, 10, 15, 20, at.%) alloys and determined that the Mg−15Ni−3La alloy had the lowest hydrogen desorption activation value (E_a) of 80.36 kJ/mol. ZHANG et al [20] studied nanocrystalline and amorphous $LaMg_{11}Ni$+x% Ni (x=100, 200, mass fraction) alloys by mechanical milling and found that increasing Ni content visibly improves the gaseous hydrogen storage properties. SPASSOV and KÖSTER [21] prepared a series of Mg−Ni−RE alloys (RE=La, Ce, Y) with nanocrystalline and amorphous or partially amorphous microstructures by rapid quenching and the as-quenched $Mg_{75}Ni_{20}Mm_5$ (Mm=Ce, La-rich misch metal) alloy could absorb 4.0 wt.% H_2 in 100 min. YUAN et al [22] reported the effect of Mm content on the microstructure and hydrogen storage properties of the as-cast Mg−10Ni−xMm (x=1, 2, 3, at.%) in which alloys were prepared using a simple one-step method of induction melting. The amount of hydrogen absorption reached 5.26 wt.% within 350 s at 573 K and the hydrogen desorption amount reached 4.72 wt.% in less than 300 s at the same temperature. The E_a value of MgH_2 in this system was decreased to 88.6 kJ/mol. These studies reveal that RE−Mg−Ni alloys have good hydrogen absorption and desorption properties, and thus deserve additional examination.

LIU et al [23] reported that $Mg_{100-x}Ni_x$ (x=5, 11.3, 20, 25) specimens have excellent hydrogen storage properties but did not consider alloying methods. Considering that the addition of rare-earth elements can enhance hydrogen storage performance, the target materials were determined to be $La_5Mg_{95-x}Ni_x$ (x=5, 10, 15). In this study, changes in the microstructure, hydrogen storage kinetics, and thermodynamics performance of $La_5Mg_{95-x}Ni_x$ (x=5, 10, 15) ternary alloys, which were fabricated using vacuum induction melting with increasing Ni content, were systematically studied.

2 Experimental

The vacuum induction furnace was utilized to prepare $La_5Mg_{95-x}Ni_x$ (x=5, 10, 15) ternary alloys and for preventing Mg volatilizing, the furnace was put in a helium atmosphere. The source of He is from CISRI corporation, and its purity is at least 99.999%. In the preparation conditions, putting excess Mg (10%) and La (5%) is crucial to compensate for evaporative loss based on our experience. After the alloys were melted, insulation for 10 min made them well mixed, then molten alloys were poured into a copper cooled mould. When cooling to room temperature, a cast ingot was obtained.

X-ray diffraction (D/max/2400) was utilized to determine the phase structures of as-milled alloys. The experimental parameters were set as 160 mA, 40 kV and 10 (°)/min, and it was performed with Cu $K_{\alpha 1}$ radiation filtered by graphite. The morphologies of the as-cast $La_5Mg_{95-x}Ni_x$ (x=5, 10, 15) alloys were observed using A Philips SEM (QUANTA 400).

The P−C−I curves, hydrogen absorption and desorption kinetics of $La_5Mg_{95-x}Ni_x$ (x=5, 10, 15) ternary alloys were measured by an automatically controlled Sieverts apparatus produced by Suzuki Shokan Co., Ltd. (PCT−4SDWIN) with a furnace controlled to an accuracy of ±1 °C. 0.5 g sample which passed through a 300-mesh sieve was put into a cylindrical reactor in every experiment. The hydrogen absorption was conducted at an initial H_2 pressure of 3.5 MPa at 100, 150, 200, 240, 300 and 360 °C and the hydrogen desorption at an initial H_2 pressure of 1×10^{-4} MPa at 280, 300, 320, 340 and 360 °C. After every experiment, the temperature was reset to 360 °C, and the sample chamber was evacuated below 1×10^{-4} MPa for 30 min to make sure that the hydrogen was released completely. For simplification, $La_5Mg_{95-x}Ni_x$ (x=5, 10, 15) alloys are abbreviated as Mg90, Mg85 and Mg80.

3 Results and discussion

3.1 Crystal and microstructural characteristics

The X-ray diffraction (XRD) patterns of $La_5Mg_{95-x}Ni_x$ (x=5, 10, 15) ternary alloys can be seen in Fig. 1. Figure 1(a) indicates that the Mg90, Mg85, Mg80 alloys are all composed of La_2Mg_{17} as the main phase, and Mg_2Ni, La_2Ni_3 and Mg phases. However, the $LaMg_2$-based second phase is found in Mg90 and Mg85 alloys, but not in Mg80 alloy. This indicates that the amount of Mg_2Ni phase increases, whereas that of the Mg phase decreases with increasing Ni content. The actual compositions of the $La_5Mg_{95-x}Ni_x$ (x=5, 10, 15) alloys were measured by inductive coupled plasma emission spectrometer. Table 1 lists the compositions of experimental alloys.

In Fig. 1(b), XRD patterns of the alloys after hydriding show that the Mg90, Mg85 and Mg80 alloys after hydriding are all composed of MgH_2, Mg_2NiH_4 and rare earth hydride LaH_3. Combined with the previous study [24,25], we found that $La_2Mg_{17}+H_2\rightarrow LaH_3+MgH_2$, $Mg_2Ni+H_2\rightarrow Mg_2NiH_4$, and $Mg+H_2\rightarrow MgH_2$ occurred in Mg90, Mg85, and Mg85 alloys during the first hydrogen absorption. Moreover, $LaMg_2+H_2\rightarrow LaH_3+MgH_2$ also occurred in Mg90 and Mg85.

From Fig. 1(c), the XRD patterns of the alloys after dehydriding show that the Mg90, Mg85, and Mg80 alloys after dehydriding are all composed of Mg_2Ni, Mg and rare earth hydride LaH_3. This indicates that MgH_2

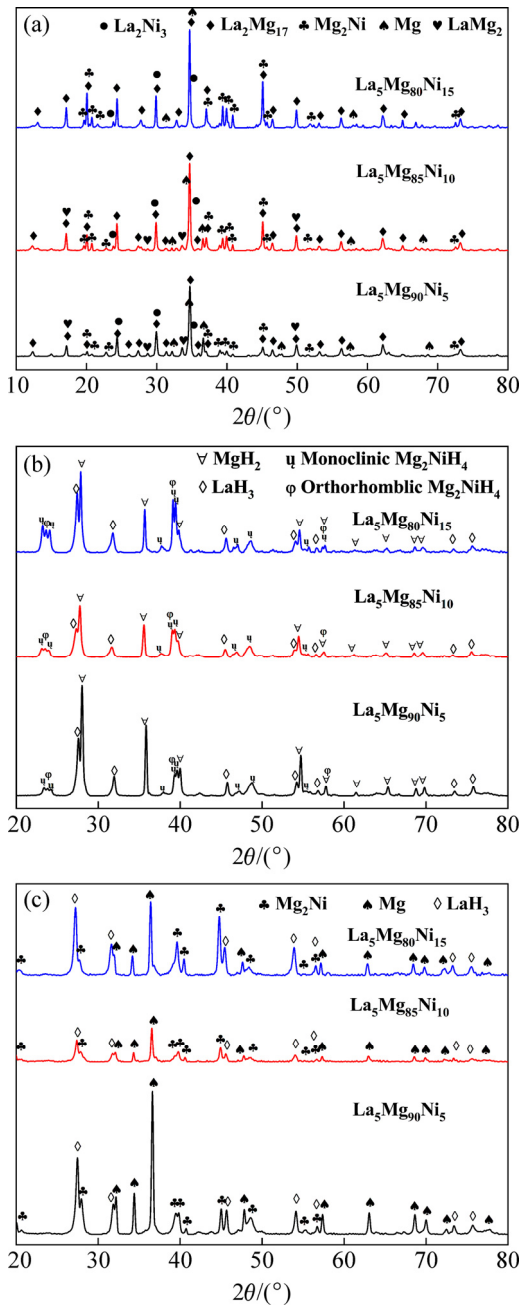

Fig. 1 XRD patterns of $La_5Mg_{95-x}Ni_x$ (x=5, 10, 15) alloys: (a) As-cast; (b) After hydriding; (c) After dehydriding

Table 1 Actual compositions (wt.%) of $La_5Mg_{95-x}Ni_x$ (x=5, 10, 15) alloys measured by ICP

Alloy	La	Mg	Ni
Mg90	21.87±0.20	68.89±0.27	9.24±0.03
Mg85	20.75±0.19	61.72±0.24	17.53±0.02
Mg80	19.73±0.22	55.24±0.25	25.02±0.05

and Mg_2NiH_4 transform into Mg and Mg_2Ni during the dehydrogenation process, whereas the rare earth hydride LaH_3 is difficult to disintegrate. The rare earth hydride LaH_3 phase is unable to participate in reversible hydrogen absorption and desorption, due to its higher decomposition temperature. It is inferred that the reactions occurring during hydrogen absorption and desorption are $Mg+H_2 \leftrightarrow MgH_2$ and $Mg_2Ni+H_2 \leftrightarrow Mg_2NiH_4$.

For observing the microstructures of $La_5Mg_{95-x}Ni_x$ (x=5, 10, 15) ternary alloys, Fig. 2 shows back-scattered SEM images. It is indicated that the microstructure has great changes with the rising of Ni content. According to the EDS and Mg−Ni−La ternary phase diagram [26], the alloys are all composed of four phases. The dark region

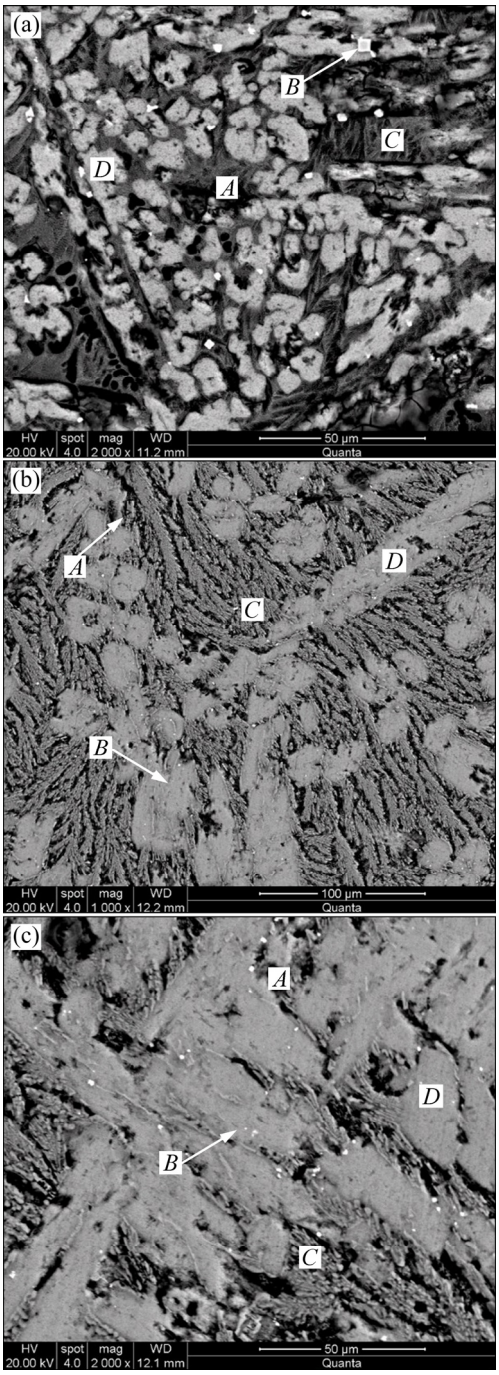

Fig. 2 Back-scattered SEM images of $La_5Mg_{95-x}Ni_x$ (x=5, 10, 15) ternary alloys: (a) x=5; (b) x=10; (c) x=15

is Mg, the bright region is Mg_2Ni, the dark gray region is $LaMg_x$ ($LaMg_2$ + Mg + La_2Mg_{17}), and the shiny gray region is $LaMg_x$ + Mg_2Ni, represented by *A*, *B*, *C*, *D* in the images. It is shown that the microstructure of $LaMg_x$ changes from reticular to planar, and the amount of Mg_2Ni phase increases considerably, whereas the Mg phase gradually disappears with the rising of Ni content.

Scanning electron microscopy (SEM) images of the powders before and after hydriding are shown in Fig. 3, with Mg90 as representative. Figures 3(a) and (b) shows that the surface of the powder particles is smooth before hydriding. However, many cracks are produced after hydriding, as shown in Figs. 3(c) and (d). These cracks are produced by the accumulation of internal stresses caused by the constant expansion and contraction of unit cells during the hydrogen absorption/desorption process. The cracks can provide diffusion paths for hydrogen atoms, which help to improve the hydrogen storage performance of the alloys.

Figure 4 shows isothermal hydrogenation and dehydrogenation curves for $La_5Mg_{95-x}Ni_x$ (x=5, 10, 15) ternary alloys. Hydrogenation activation and the dehydrogenation reaction occur at 360 °C and 3.5 MPa and at 360 °C and 1×10^{-4} MPa, respectively. With more than five activation cycles, the Mg90, Mg85 and Mg80 alloys have 5.8, 5.3 and 4.9 wt.% reversible hydrogen absorption/desorption capacity, respectively. Clearly, the capacity reduces with increasing Ni content because the hydrogen absorption/desorption capacity of Mg is much greater than that of Mg_2Ni. Meanwhile, the capacity of each alloy hardly changes as the cycles are increased. Moreover, the maximum capacities of Mg90, Mg85, and Mg80 during the first absorption activation process are 6.4, 5.9 and 5.5 wt.%, respectively, which are greater than the reversible capacities.

This phenomenon is due to the fact that rare earth hydride LaH_3 is difficult to disintegrate during the desorption process because of its high thermal stability. Regarding the first desorption process, 246, 180 and 144 s are considered for Mg90, Mg85 and Mg80 alloys, respectively, to reach complete desorption activation. After reaching a stable state, Mg90, Mg85 and Mg80 require 192, 156 and 120 s, respectively, to reach complete desorption activation. As shown in Fig. 4, Mg90 reaches complete activation after five cycles, whereas Mg85 and Mg90 reach it after only three cycles. The activation is significantly reduced with increasing Ni content.

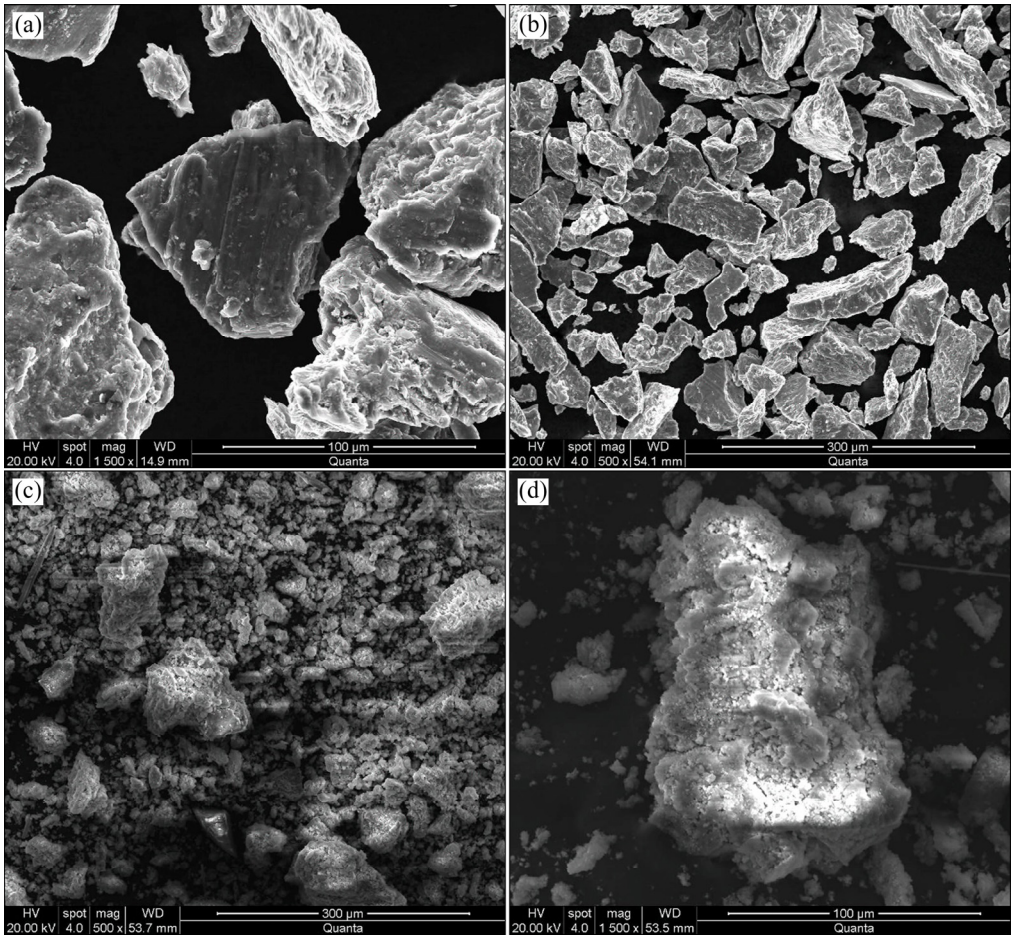

Fig. 3 SEM images of powders of $La_5Mg_{90}Ni_5$: (a, b) Before hydriding; (c, d) After hydriding

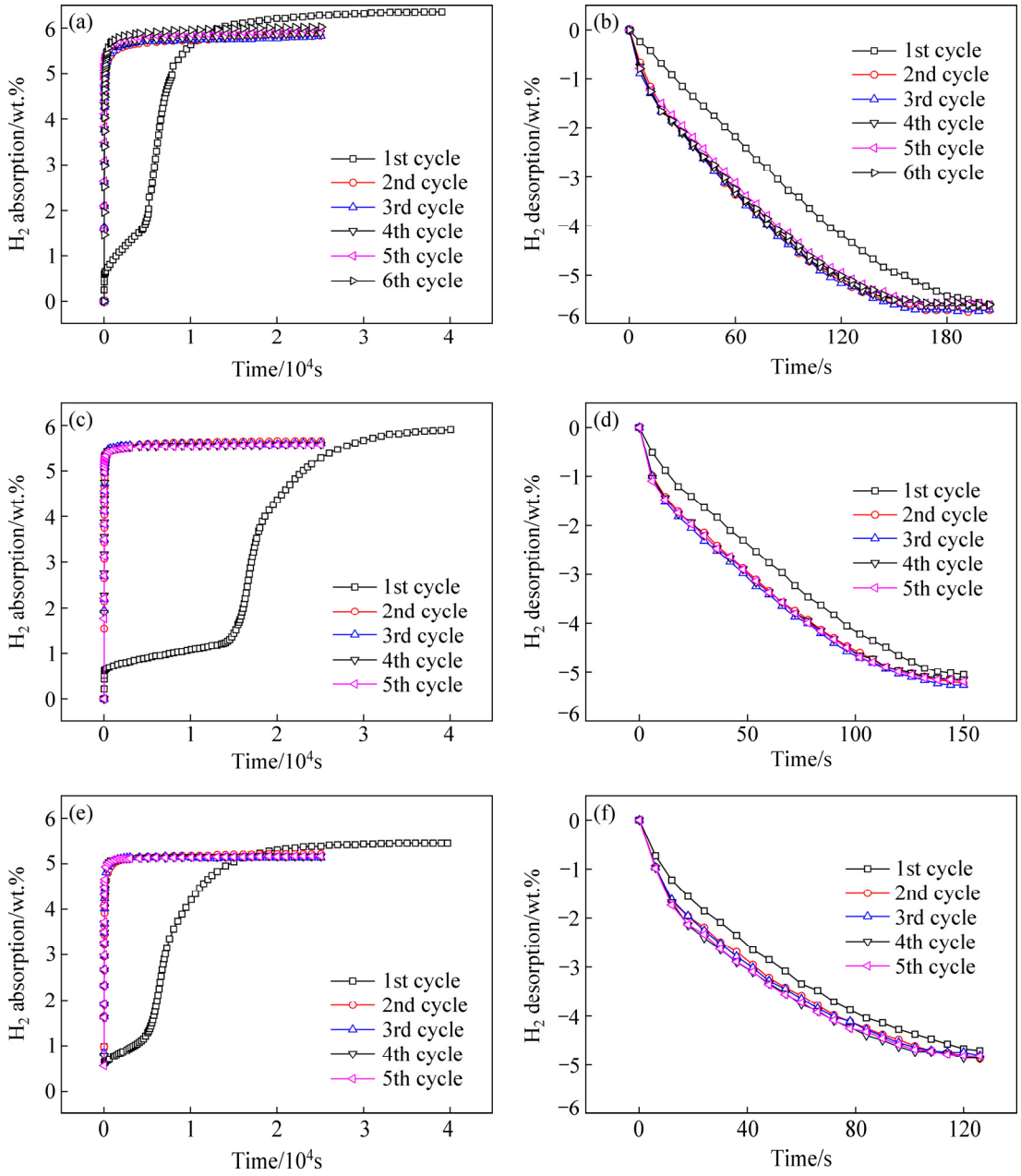

Fig. 4 Isothermal hydrogen absorption and desorption curves of $La_5Mg_{95-x}Ni_x$ (x=5, 10, 15) alloys in cycle activation with hydrogenation reaction at 360 °C and 3.5 MPa (a, c, e), and dehydrogenation reaction at 360 °C and 1×10^{-4} MPa (b, d, f): (a, b) x=5; (c, d) x=10; (e, f) x=15

3.2 Hydrogen storage kinetics

The isothermal hydrogen absorption/desorption kinetic curves are shown in Figs. 5 and 6. Clearly, the hydrogen absorption rate and capacity of the alloys increase remarkably with rising temperature. Moreover, although the reversible hydrogen capacity decreases with increasing Ni content, the rate notably increases. The curves at 100 °C and particularly at 150 °C show that the absorption rate increases with increasing Ni content. This means that Ni remarkably improves hydrogen storage kinetics in the experimental range.

As seen from Fig. 6, the dehydrogenation capacities also decrease with increasing Ni content. To complete dehydrogenation at 360, 340, 320, 300 and 280 °C, Mg90 requires 192, 252, 450, 684 and 2760 s, respectively, Mg85 requires 156, 204 384, 600 and 960 s, respectively, and Mg80 requires 120, 156, 216, 343 and 660 s, respectively. Clearly, the dehydrogenation rate increases with increasing Ni content, and Ni remarkably improves the hydrogen storage kinetics of alloys. The Johnson−Mehl−Avrami (JMA) model was utilized to simulate the curves related to hydrogen storage kinetics and hydrogen desorption activation, and the Arrhenius method was employed to calculate the critical value.

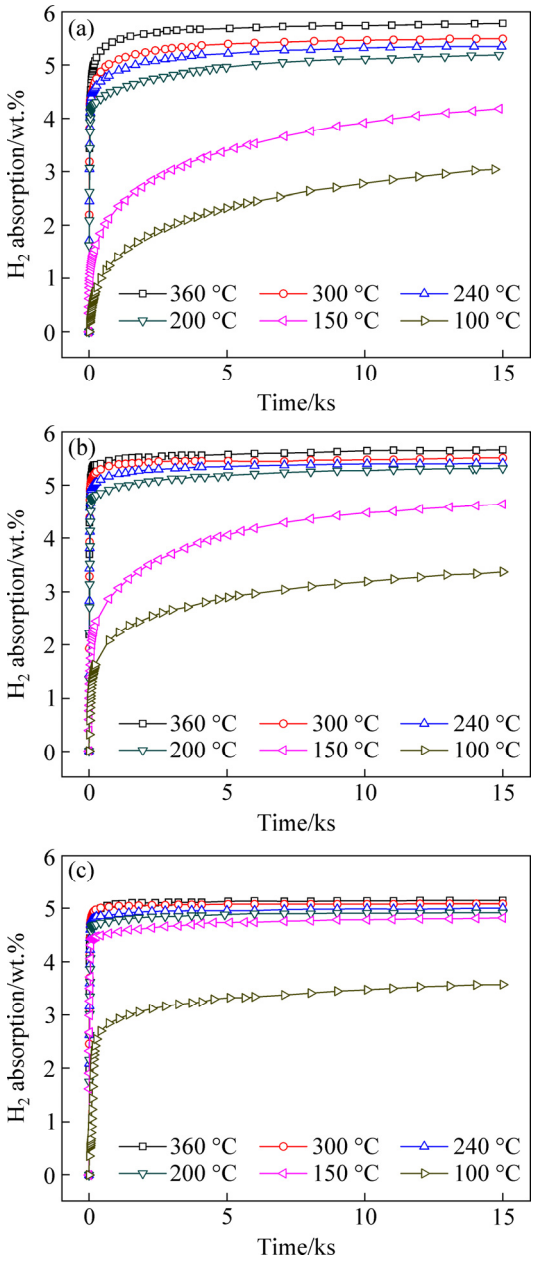

Fig. 5 Isothermal hydrogenation kinetic curves of $La_5Mg_{95-x}Ni_x$ (x=5, 10, 15) alloys at different temperatures: (a) x=5; (b) x=10; (c) x=15

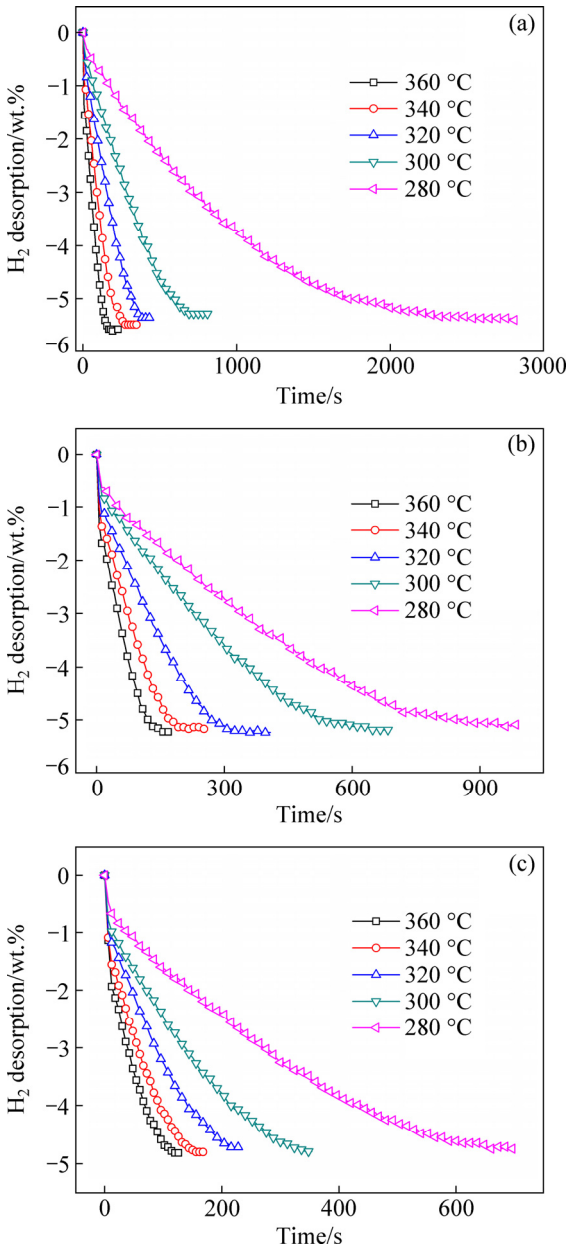

Fig. 6 Isothermal dehydrogenation kinetic curves of $La_5Mg_{95-x}Ni_x$ (x=5, 10, 15) alloys at different temperatures: (a) x=5; (b) x=10; (c) x=15

Then, the influence of Ni content on the hydrogen storage kinetics could be obtained from the results. In general, activation energy is seen as an obstacle in which all potential barriers that perform a gas−solid reaction must be overcome, as activation energy is an extremely critical part of gas−solid reaction kinetics. It is widely acknowledged that hydrogen desorption reactions are related to total energy barriers, which must be considered in hydrogen desorption processes. The JMA model can be used to simulate the nucleation and growth processes of the alloys:

$$\ln[-\ln(1-\alpha)]=\eta\ln k+\eta\ln t \quad (1)$$

where t, α, η and k characterize the time, the fraction of the alloy converted to hydride at time t, the Avrami exponent, and an effective kinetic parameter. As seen from Fig. 7, by utilizing the logarithmic transformation, we can obtain JMA curves of $\ln[-\ln(1-\alpha)]$ and $\ln t$ at 320, 340 and 360 °C for the dehydrogenation of alloys. The JMA curves are found to be nearly linear, which means that the dehydriding reaction of the alloys is activated by instantaneous nucleation, which is followed by an interface-controlled three-dimensional growth process. The value of k can be obtained from the slope η and intercept $\eta\ln k$. Arrhenius methods can be then used to calculate the E_a:

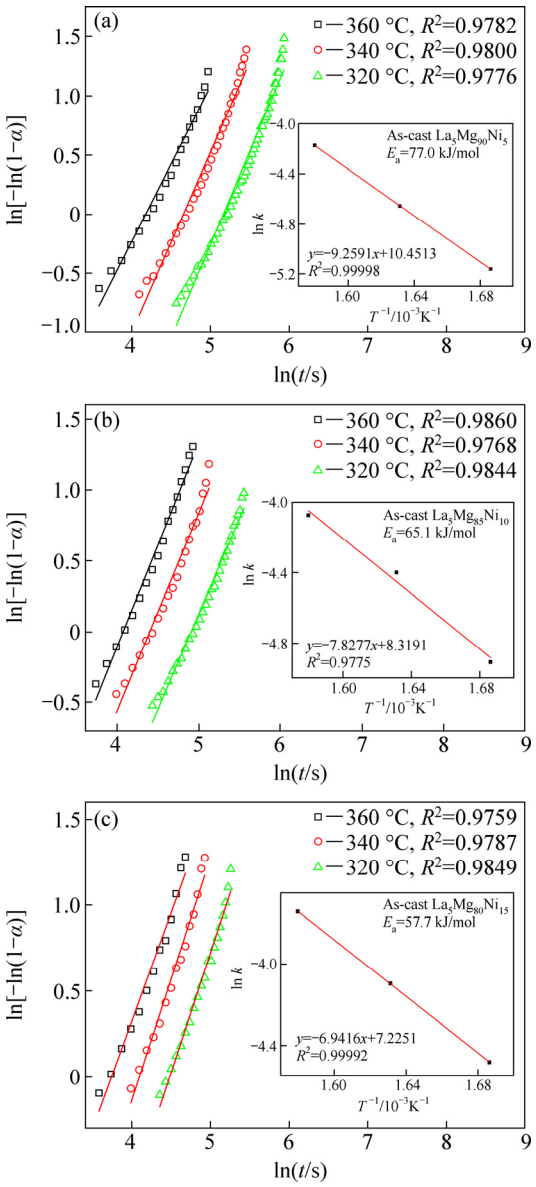

Fig. 7 JMA plots and Arrhenius plots for dehydrogenation of $La_5Mg_{95-x}Ni_x$ (x=5, 10, 15) alloys: (a) x=5; (b) x=10; (c) x=15

$$k=A\exp[-E_a/(RT)] \quad (2)$$

where A, R and T characterize a temperature independent coefficient, the universal gas constant, and an absolute temperature. As seen from Fig. 7, by utilizing the logarithmic transformation, we can obtain Arrhenius curves of ln k and $1/T$ at 320, 340, and 360 °C for the dehydrogenation of alloys. The Arrhenius curves are found to be nearly linear and the E_a values of the alloys can be calculated by the slopes of the line. The E_a values of Mg90, Mg85 and Mg80 are calculated as 77.0, 65.1 and 57.7 kJ/mol, respectively. In addition, hydrogen storage kinetics is improved with increasing Ni content. The value is considerably lower than 150−160 kJ/mol of the MgH_2 [27,28] and 80.36 kJ/mol of Mg−15Ni−3La alloy [19], but approximates 59.1−78.6 kJ/mol of the $LaMg_{11}Ni$+xNi alloy [20]. The lower E_a value is mostly the result of alloying and the presence of the rare earth hydride. The addition of Ni causes the alloy to produce more Mg_2Ni, whereas Mg_2Ni has very low hydrogen evolution activation energy, even though its hydrogen storage capacity is less than that of Mg. Moreover, adding the rare earth La causes the activated alloy to produce a rare earth hydride phase LaH_3, where LaH_3 has a "hydrogen pump effect" that greatly reduces the hydrogen activation energy value of the alloys.

3.3 Thermodynamic properties

The P–C–I curves of $La_5Mg_{95-x}Ni_x$ (x=5, 10, 15) ternary alloys were tested at 300, 320, 340, and 360 °C to explore the influence of Ni content on the thermodynamic properties of the alloys, as shown in Fig. 8. Two distinct

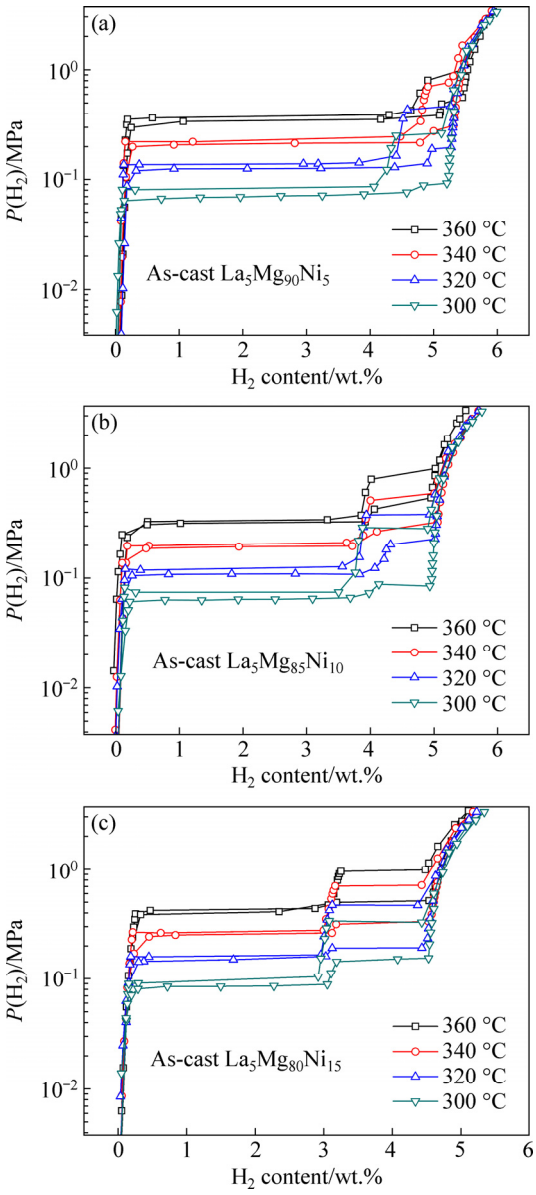

Fig. 8 P–C–I curves of $La_5Mg_{95-x}Ni_x$ (x=5, 10, 15) alloys measured at different temperatures: (a) x=5; (b) x=10; (c) x=15

hydrogen absorption/desorption plateaus can be clearly seen on the *P*−*C*−*I* curves. The reactions at the first and second absorption plateaus are $Mg+H_2 \rightarrow MgH_2$ and $Mg_2Ni+H_2 \rightarrow Mg_2NiH_4$, respectively, according to XRD. A slight slope appears on the upper plateau because Mg_2Ni phase undergoes internal stress, particularly in the Mg90 alloy. The XRD patterns show obvious diffraction peaks of Mg_2Ni. In addition, the *P*−*C*−*I* curves reveal that the critical thermodynamic parameters of $La_5Mg_{95-x}Ni_x$ (x=5, 10, 15) ternary alloys, namely, ΔH and ΔS, are easily calculated using the van't Hoff equation:

$$\ln[P(H_2)/P_0]=\Delta H/(RT)-\Delta S/R \quad (3)$$

where $P(H_2)$ and P_0 characterize the equilibrium plateau pressure and 1.01325×10^5 Pa, respectively. Figure 9 shows the van't Hoff curves of $[P(H_2)/P_0]$ and $1/T$. The curves are found to be nearly linear, where the ΔH and ΔS values can be estimated by the slopes and intercepts of the line. The ΔH and ΔS values of Mg90, Mg85 and Mg80 are calculated to be −74.4, −72.1, −73.0 kJ/mol and −128.2, −123.2, −126.8 J/(mol·K), respectively. It is found that both the ΔH and ΔS values initially decrease and then increase with increasing Ni content. We can see that the ΔH for the alloys is slightly lower than −78.6 kJ/mol of pure Mg [25,26], −82.1 kJ/mol of the Mg−Ni−La composite powders (Mg:Ni:La=85:10:5 in mass ratio) [29], and −76.12 kJ/mol of $PrMg_{11}Ni$ [30], and approximates −74.0 kJ/mol of Mg−5Ni−3Ni (at.%) [31]. This indicates that the thermodynamic properties of the alloys initially increase and then decrease with increasing Ni content in this range, which means that alloying enhances the thermodynamic properties. The excellent performance is mostly due to the proper mixing ratio, the microstructure of the alloy, and the presence of the rare earth hydride.

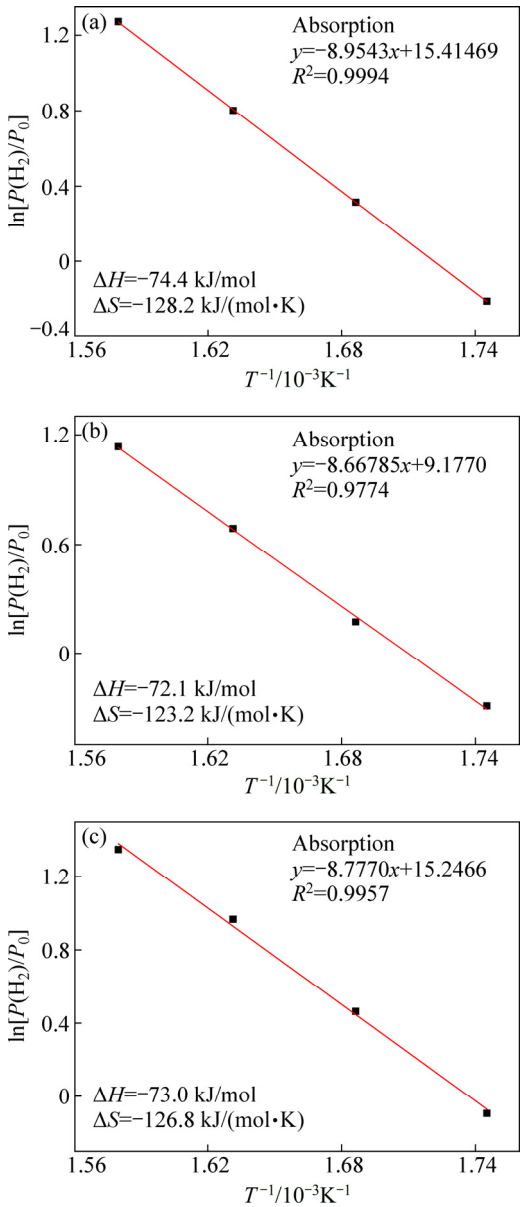

Fig. 9 van't Hoff plots of $La_5Mg_{95-x}Ni_x$ (x=5, 10, 15) alloys measured at different temperatures: (a) x=5; (b) x=10; (c) x=15

4 Conclusions

(1) The as-cast Mg90, Mg85 and Mg80 alloys are all composed of La_2Mg_{17} as the main phase, Mg_2Ni, La_2Ni_3 and Mg second phases, whereas $LaMg_2$ is only found in Mg90 and Mg85 alloys. The amount of Mg_2Ni increases as the amount of Mg decreases with increasing Ni content. The alloys after hydriding are all composed of MgH_2, Mg_2NiH_4 and the rare earth hydride LaH_3, whereas those after dehydriding are all composed of Mg_2Ni, Mg and rare earth hydride LaH_3. We can infer that the reactions that occur during hydrogen absorption and desorption are $Mg+H_2 \leftrightarrow MgH_2$ and $Mg_2Ni+H_2 \leftrightarrow Mg_2NiH_4$, respectively.

(2) The increased Ni content remarkably improves the hydrogen storage kinetic performance of the alloys but reduces their hydrogen absorption/desorption capacity. The Mg80 alloy shows the lowest E_a value of 57.7 kJ/mol and the highest hydrogen absorption/desorption rate.

(3) The thermodynamic properties are initially improved and then degraded with increasing Ni content. These changes are caused by the proper mixing ratio, the microstructure of the alloy, and the presence of the rare earth hydride. The Mg85 alloy is proven to have the best thermodynamic properties with ΔH of −72.1 kJ/mol and ΔS of −123.2 J/(mol·K).

References

[1] DONG Bao-xiang, GAO Jing-jing, TENG Yun-lei, TIAN Hui, WANG Long-zheng. A novel hydrogen storage system of $KLi_3(NH_2)_4$−4LiH with superior cycling stability [J]. International Journal of Hydrogen Energy, 2016, 41: 5371−5377.

[2] ZHANG Yang-huan, ZHANG Wei, SONG Xi-ping, ZHANG

Pei-long, ZHU Yong-guo, QI Yan. Effects of spinning rate on structures and electrochemical hydrogen storage performances of RE−Mg−Ni−Mn-based AB_2-type alloys [J]. Transactions of Nonferrous Metals Society of China, 2016, 26: 3219−3231.

[3] İSKENDER M, ATIŞ M. Boron-doped hydrogenated Al3 clusters: A material for hydrogen storage [J]. Journal of Alloys & Compounds, 2016, 667: 275−281.

[4] CAPPILLINO P J, LAVERNIA E J, ONG M D, YANG N Y. Plastic deformation and hysteresis for hydrogen storage in Pd−Rh alloys [J]. Journal of Alloys & Compounds, 2014, 586: 59−65.

[5] WU Zhen, ZHANG Zao-xiao, YANG Fu-sheng, FENG Peng-hui, WANG Yu-qi. Hydrogen storage properties and mechanisms of magnesium-based alloys with mesoporous surface [J]. International Journal of Hydrogen Energy, 2016, 41: 2771−2780.

[6] ANIK M, KARANFIL F, KÜÇÜKDEVECI N. Development of the high-performance magnesium-based hydrogen storage alloy [J]. International Journal of Hydrogen Energy, 2012, 37: 299−308.

[7] ZHANG Yang-huan, HAN Zhong-gang, YUAN Ze-ming, YANG Tai, QI Yan, ZHAO Dong-liang. Electrochemical properties of nanocrystalline and amorphous Mg−Y−Ni alloys applied to Ni−MH battery [J]. Transactions of Nonferrous Metals Society of China, 2015, 25: 3736−3746.

[8] JAIN I P, LAL C, JAIN A. Hydrogen storage in Mg: A most promising material [J]. International Journal of Hydrogen Energy, 2010, 35: 5133−5144.

[9] OESTERREICHER H, BITTNER H. Hydride formation in $La_{1-x}Mg_xNi_2$ [J]. Journal of the Less-Common Metals, 1980, 73: 339−344.

[10] KOHNO T, YOSHIDA H, KAWASHIMA F, INABA T, SAKAI I, KANDA M. Hydrogen storage properties of new ternary system alloys: La_2MgNi_9, $La_5Mg_2Ni_{23}$, La_3MgNi_{14} [J]. Journal of Alloys and Compounds, 2000, 311: 5−7.

[11] LASS E A. Hydrogen storage measurements in novel Mg-based nanostructured alloys produced via rapid solidification and devitrification [J]. International Journal of Hydrogen Energy, 2011, 36: 10787−10796.

[12] XIE Li-shuai, LI Jin-shan, ZHANG Tie-bang, KOU Hong-chao. De/hydrogenation kinetics against air exposure and microstructure evolution during hydrogen absorption/desorption of Mg−Ni−Ce alloys [J]. Renewable Energy, 2017, 113: 6118−6126.

[13] ZHANG Yang-huan, YANG Tai, BU Wen-gang, CAI Ying, ZHANG Gong-fang, ZHAO Dong-liang. Effect of Nd content on electrochemical performances of nanocrystalline and amorphous $(Mg_{24}Ni_{10}Cu_2)_{100-x}Nd_x$ (x=0−20) alloys prepared by melt spinning [J]. Transactions of Nonferrous Metals Society of China, 2013, 23: 3668−3676.

[14] ZHANG Qing-an, JIANG Chang-jie, LIU Dong-dong. Comparative investigations on the hydrogenation characteristics and hydrogen storage kinetics of melt-spun $Mg_{10}NiR$ (R=La, Nd and Sm) alloys [J]. International Journal of Hydrogen Energy, 2012, 37: 10709−10714.

[15] KALINICHENKA S, RÖNTZSCH L, RIEDL T, WEIßGÄRBER T, KIEBACK B. Hydrogen storage properties and microstructure of melt-spun $Mg_{90}Ni_8RE_2$ (RE=Y, Nd, Gd) [J]. International Journal of Hydrogen Energy, 2011, 36: 10808−10815.

[16] KALINICHENKA S, RÖNTZSCH L, RIEDL T, GEMMINGC T, WEIßGÄRBER T, KIEBACK B. Microstructure and hydrogen storage properties of melt-spun Mg−Cu−Ni−Y alloys [J]. International Journal of Hydrogen Energy, 2011, 36: 1592−1600.

[17] KALINICHENKA S, RÖNTZSCH L, BAEHTZ C, KIEBACK B. Hydrogen desorption kinetics of melt-spun and hydrogenated $Mg_{90}Ni_{10}$, and $Mg_{80}Ni_{10}Y_{10}$, using in situ synchrotron, X-ray diffraction and thermogravimetry [J]. Journal of Alloys & Compounds, 2010, 496: 608−613.

[18] HAO Gu, ZHU Yun-feng, LI Li-quan. Effect of La/Ni ratio on hydrogen storage properties of Mg−Ni−La system prepared by hydriding combustion synthesis followed by mechanical milling [J]. International Journal of Hydrogen Energy, 2008, 33: 2970−2974.

[19] LV Yu-jie, ZHANG Bao, WU Ying. Effect of Ni content on microstructural evolution and hydrogen storage properties of Mg−xNi−3La (x=5, 10, 15, 20 at.%) alloys [J]. Journal of Alloys & Compounds, 2015, 641: 176−180.

[20] ZHANG Yang-huan, LI Long-wen, FENG Dian-chen, GONG Peng-fei, SHANG Hong-wei, GUO Shi-hai. Hydrogen storage behavior of nanocrystalline and amorphous La−Mg−Ni−based $LaMg_{12}$−type alloys synthesized by mechanical milling [J]. Transactions of Nonferrous Metals Society of China, 2017, 27: 551−561.

[21] SPASSOV T, KÖSTER U. Hydrogenation of amorphous and nanocrystalline Mg-based alloys [J]. Journal of Alloys & Compounds, 1999, 287: 243−250.

[22] YUAN Jiang-guang, XING Na, WU Ying. The effect of Mm content on microstructure and hydrogen storage properties of the as-cast Mg−10Ni−xMm (x=1, 2, 3 at.%) alloys [J]. International Journal of Hydrogen Energy, 2016, 42: 6118−6126.

[23] LIU Xiao-feng, ZHU Yun-feng, LI Li-quan. Hydrogen storage properties of $Mg_{100-x}Ni_x$ (x=5, 11.3, 20, 25) composites prepared by hydriding combustion synthesis followed by mechanical milling (HCS + MM) [J]. Intermetallics, 2007, 15: 1582−1588.

[24] ZHANG Yang-huan, YUAN Ze-ming, BU Wen-gang, HU Feng, CAI Ying, ZHAO Dong-liang. Hydrogen storage thermodynamics and dynamics of Nd−Mg−Ni-Based $NdMg_{12}$-type alloys synthesized by mechanical milling [J]. Acta Metallurgica Sinica (English Letters), 2016, 29: 1−10.

[25] YANG Tai, YUAN Ze-ming, BU Wen-gang, JIA Zhi-chao, QI Yan, ZHANG Yang-huan. Effect of elemental substitution on the structure and hydrogen storage properties of $LaMgNi_4$ alloy [J]. Materials & Design, 2016, 93: 46−52.

[26] WEST D R F. Ternary alloys—A comprehensive compendium of evaluated constitutional data and phase diagrams [M]. Stuttgart, VCH, 1995.

[27] STAMPFER J F Jr, HOLLEY C E, SUTTLE J F. The magnesium-hydrogen system 1−3 [J]. Journal of the American Chemical Society, 1960, 82: 3504−3508.

[28] VIGEHOLM B, KJØLLER J, LARSEN B. Magnesium for hydrogen storage [J]. Journal of the Less-Common Metals, 1980, 74: 205−211.

[29] ZOU Jian-xin, GUO Hao, ZENG Xiao-qin, ZHOU Si, CHEN Xi, DING Wen-jiang. Hydrogen storage properties of Mg−TM−La (TM=Ti, Fe, Ni) ternary composite powders prepared through arc plasma method [J]. International Journal of Hydrogen Energy, 2013, 38: 8852−8862.

[30] ZHANG Yang-huan, LI Ya-qin, SHANG Hong-wei, YUAN Ze-ming, CAI Ying, QI Yan, ZHAO Dong-liang. Hydrogen storage properties of nanocrystalline and amorphous Pr−Mg−Ni−based alloys synthesized by mechanical milling [J]. International Journal of Hydrogen Energy, 2017, 42: 22379−22387.

[31] ZHANG Bao, LV Yu-jie, YUAN Jiang-guang, WU Ying. Effects of microstructure on the hydrogen storage properties of the melt-spun Mg−5Ni−3La (at.%) alloys [J]. Journal of Alloys & Compounds, 2017, 702: 126−131.

$La_5Mg_{95-x}Ni_x$ (x=5、10、15)合金的显微组织、储氢热力学和动力学性能

李振阳[1,2]，李胜利[1]，袁泽明[2,3]，张羊换[2,3]，祁 焱[2]

1. 山东大学 材料科学与工程学院，济南 250061；
2. 钢铁研究总院 功能材料研究所，北京 100081；
3. 内蒙古科技大学 内蒙古自治区白云鄂博矿多金属资源综合利用重点实验室，包头 014010

摘 要：研究 Ni 含量对 $La_5Mg_{95-x}Ni_x$(x=5、10、15)三元合金的显微组织、热力学和动力学性能的影响。采用 XRD 和 SEM 探索合金的相和组织的变化情况，采用自动 Sievert 设备测试合金吸放氢性能曲线和 PCI 曲线。研究表明，随着 Ni 含量的增加，合金的储氢动力学性能得到提高，但是合金的储氢容量有所下降。三种成分的合金中，$La_5Mg_{80}Ni_{15}$ 合金表现出最低的放氢活化能以及最高的吸放氢速率，其放氢活化能为 57.7 kJ/mol。通过测定合金 PCI 曲线和 van't Hoff 方程发现，随着 Ni 含量的增加，合金的热力学性能先提高后降低，其中 $La_5Mg_{85}Ni_{10}$ 表现出最优异的热力学性能，其焓和熵的数值分别为−72.1 kJ/mol 和−123.2 J/(mol·K)。

关键词：储氢；镁基合金；热力学性能；动力学性能；Ni 含量

(Edited by Bing YANG)